Luo et al. Nanoscale Research Letters (2018) 13:282
https://doi.org/10.1186/s11671-018-2696-x

Nanoscale Research Letters

NANO EXPRESS Open Access

Adsorption of Transition Metals on Black Phosphorene: a First-Principles Study

Yi Luo[1], Chongdan Ren[2], Sake Wang[3], Shaohan Li[1], Peigen Zhang[1], Jin Yu[1*], Minglei Sun[4,5*], Zhengming Sun[1] and Wencheng Tang[4]

Abstract

Black phosphorene is a novel two-dimensional material which has unique properties and wide applications. Using first-principles calculations, we investigated the adsorption behavior of 12 different transition metals (TMs; Fe, Co, Ni, Cu, Ru, Rh, Pd, Ag, Os, Ir, Pt, and Au) on phosphorene. Our results showed that all of the adsorption systems have a large binding energy. The Fe-, Co-, and Au-phosphorene systems display magnetic states with magnetic moments of 2, 1, and 0.96 μ_B, respectively, which means that these systems are magnetic semiconductors. Adsorption of oxygen molecules on TM-phosphorene was also investigated. Interestingly, all the O_2-(TM-phosphorene) systems, except O_2-(Pd-phosphorene), can elongate the O–O bond, which is critical to their application as catalysts in the oxidation of CO. We also found that the adsorption of O_2 molecules enables the O_2-(Fe-, Ni-, Cu-, Ir-, Rh-, Ag-, and Au-phosphorene) systems to become magnetic semiconductors, and it allows O_2-(Co-phosphorene) to display half-metallic state. Our results are expected to have important implications for phosphorene-based catalysis and spintronics.

Keywords: Black phosphorene, Adsorption, Half-metal, Spintronics, CO oxidization, Catalyst

Background

Phosphorene [1–3], a monolayer of phosphorus atoms arranged in a puckered honeycomb structure, has unique properties which include a direct semiconducting nature [4], ultrahigh mobility at room temperature [4–6], superior mechanical flexibility [7], and high thermoelectric performance [8–10]. These properties make phosphorene a very suitable material for a variety of applications such as field-effect transistors [1, 11–16], Li- and Na-ion batteries [17–19], solar cells [20, 21], photocatalysts [22], spintronics [23], and gas sensors [24–26]. However, phosphorene is a nonmagnetic material, and some strategies must be adopted to widen its application.

For two-dimensional (2D) materials, adsorption is usually selected as the approach to induce magnetism for specific applications. Previously, Cao et al. [27] showed that the electronic and magnetic properties of graphene can be effectively modulated by adatoms of Fe, Co, Ni, and Cu. Kaloni et al. [28] demonstrated that magnetic moments can be induced in Ti-, V-, Cr-, Mn-, Fe-, and Co-decorated silicene systems using first-principles calculations. Ersan et al. [29] found that *b*-Arsenene displayed spin-polarized characters after adsorption of H, B, C, P, Ge, As, and Sb atoms. Furthermore, *w*-Arsenene can attain net magnetic moments with the adatoms of H, B, N, P, Cl, Ti, As, and Sb. For black phosphorene, Kulish et al. [30] predicted that Ag-, Au-, Ti-, V-, Cr-, Mn-, Fe-, and Co-phosphorene are rather stable, and a diverse range of magnetic moments can be induced in theoretical calculations. Moreover, the properties of different types of charge carriers can also be tuned by adsorbing different atoms on phosphorene. Ding and Wang [31] used the first-principles calculations to systematically illustrate the structural, electronic, and magnetic properties of atoms adsorbed on phosphorene. They noted that adatoms can introduce magnetism in phosphorene, with P, Co, and Au adatoms inducing stable magnetic properties. Hu and Hong [32] used the first-principles calculations to demonstrate the magnetic properties of metal adatoms on phosphorene; they

* Correspondence: yujin@seu.edu.cn; sunsunminglei@gmail.com
[1]Jiangsu Key Laboratory of Advanced Metallic Materials, School of Materials Science and Engineering, Southeast University, Nanjing 211189, Jiangsu, People's Republic of China
[4]School of Mechanical Engineering, Southeast University, Nanjing 211189, Jiangsu, People's Republic of China
Full list of author information is available at the end of the article

showed that magnetism can be obtained in phosphorene by adsorbing Cr, Fe, Co, or Au atoms on its surface. Furthermore, they predicted that the Fe-phosphorene adsorption system will be a promising dilute magnetic semiconducting material. Thus, the adsorption of transition metals (TMs) on black phosphorene can be expected to effectively tune the magnetic properties of the material.

Although the above investigations studied the adsorption behavior of transition metals on black phosphorene, some issues remain unresolved. For instance, previous studies mainly focused on the properties of 3d TMs adsorbed on phosphorene. How will 4d and 5d TMs engineer the properties of phosphorene? In addition, noble metals absorbed on phosphorene can also be used as single-atom catalysts. Li et al. [33] suggested that silicene with adsorbed Au can be a high-activity catalyst with low catalytic energy barriers for the oxidization of CO. Can a noble metal absorbed on phosphorene also a good candidate for the oxidization of CO? To answer these questions, we present in this paper the results of a detailed first-principles study on the structural, magnetic, and electronic properties of 12 different types of transition metal atoms adsorbed on black phosphorene. We selected elemental Fe, Co, and Ni, which are ferromagnetic metals in their bulk phase; elemental Cu, which is diamagnetic; and the noble metals Ru, Rh, Pd, Ag, Os, Ir, Pt, and Au, which are very effective for the oxidation of CO [19, 34–45]. We found that phosphorene forms strong bonds with all 12 metals, and all of the TM-phosphorene systems are rather robust. The electronic and magnetic properties of phosphorene can be effectively tuned by the adatoms. Moreover, we also found that most TM-phosphorene adsorption systems are good candidates for the catalyst in the oxidation of CO. The results of this investigation can be used for fundamental studies of phosphorene, and they can also widen its potential application in many important fields.

Methods/Experimental

Our calculations were based on spin-polarized density functional theory (DFT), and they were performed using the Vienna Ab Initio Simulation Package (VASP) [46, 47] and the generalized gradient approximation (GGA) of the Perdew-Burke-Ernzerhof (PBE) functional [48–50]. The DFT-D3 method of Grimme [51] was used to calculate the van der Waals interaction. An energy cutoff of 400 eV with a plane-wave basis set was employed. In the calculations, the atoms were relaxed until the total energy converged to 1×10^{-5} eV and the residual force on each atom was less than 0.01 eV/Å. A large supercell (4×3) along the zigzag and armchair directions was used to avoid interactions between neighboring unit cells. The lattice constants were set to a = 13.20 Å and b = 13.74 Å. We applied a vacuum space of 20 Å in the z direction to minimize the interactions between adjacent interlayers. During the optimization, a Monkhorst-Pack [52] k-point grid of $3 \times 3 \times 1$ was adopted, and a k-point grid of $7 \times 7 \times 1$ was used for the total energy calculations.

Results and Discussion

We first explored the structural properties of pristine phosphorene. Figure 1a shows the illustrations of the top and side views of the crystal structure. It can be seen that the phosphorene monolayer consists of two atomic planes, and the unit cell of phosphorene consists of four P atoms. The phosphorene monolayer has a tetragonal lattice with equilibrium lattice constants a = 3.30 Å and b = 4.58 Å. The length of the P–P bond in the horizontal direction (l_1) is 2.22 Å, while the length in the other direction (l_2) is 2.26 Å. The pristine phosphorene has a direct bandgap of 0.89 eV (Fig. 1b), with both the conduction band minimum (CBM) and the valence band maximum (VBM) located at the Γ point. The lattice constant and the bandgap we obtained highly agree with the values obtained in previous research studies [30–32, 53].

A typical adatom is always adsorbed at either one of three positions: above a hollow site (H), on a bridge (B) between two phosphorus atoms, and on top of a phosphorus atom (T). We calculated the adsorption energy of an adatom on phosphorene to examine the stability of the adsorption systems using the relationship:

$$E_{\mathrm{ad}} = \left(E_{\mathrm{TM}} + E_{\mathrm{phosphorene}}\right) - E_{\mathrm{TM-phosphorene}} \quad (1)$$

where E_{TM} is the energy of an isolated metal atom, $E_{\mathrm{phosphorene}}$ is the total energy of the pristine phosphorene

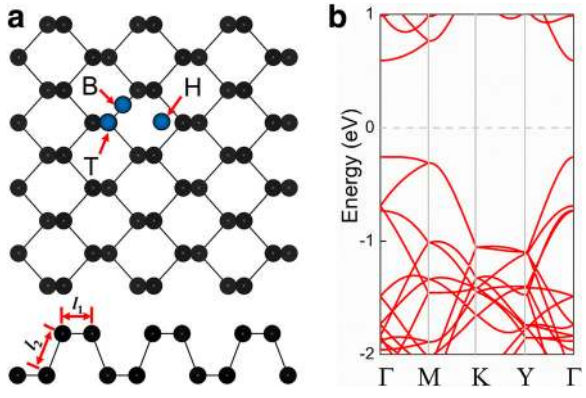

Fig. 1 **a** Top and side views of the crystal structure of pristine phosphorene ($4 \times 3 \times 1$ supercell). The blue circles represent typical positions of an impurity atom adsorbed at a hollow spot (H), on a bridge (B) between two phosphorus atoms, and on top of a phosphorus atom (T). **b** Electronic band structure and first Brillouin zone of pristine phosphorene; the Fermi level is set to zero

Table 1 Calculated minimum bond length of TM-phosphorene (d_{TM-P}), adsorption energy (E_{ad}), total magnetic moment (M_{total}), and charge transferred from TM adatom to phosphorene for a single TM atom adsorbed at the most stable adsorption site on phosphorene

Adatom	d_{TM-P} (Å)	E_{ad} (eV)	M_{total} (μ_B)	C (e)
Fe	2.16	3.254	2.00	− 0.30
Co	2.12	4.158	1.00	− 0.17
Ni	2.11	4.550	0.00	− 0.12
Cu	2.21	2.517	0.00	− 0.29
Ru	2.20	5.32	0.00	+ 0.16
Rh	2.20	5.32	0.00	+ 0.16
Pd	2.26	3.824	0.00	+ 0.07
Ag	2.43	1.465	0.00	− 0.21
Os	2.18	5.547	0.00	+ 0.17
Ir	2.19	5.969	0.00	+ 0.32
Pt	2.22	5.219	0.00	+ 0.33
Au	2.34	1.997	0.96	+ 0.16

layer, and $E_{TM\text{-}phosphorene}$ is the total energy of the adsorption system. Based on this equation, a larger adsorption energy indicates a more stable structure. We found that all the metal atoms studied in our work prefer to stay on the H site of phosphorene. The calculated adsorption energies of metal atoms adsorbed on the H site of phosphorene, shown in Table 1, vary from 2 to 6 eV. The bond length of TM-phosphorene ($d_{TM\text{-}P}$) was demonstrated to be short, in the range of 2.11–2.43 Å. Bader charge analysis [54–56] shows that 0.16, 0.16, 0.07, 0.17, 0.32, 0.33, and 0.16|e| are transferred from the Ru, Rh, Pd, Os, Ir, Pt, and Au metal atoms, respectively, to phosphorene in the (4d-TM)-phosphorene and (5d-TM)-phosphorene adsorption systems. All these results denote the formation of chemical bonds between the TM adatom and phosphorene. In addition, these results are close to recent studies [30–32].

As shown in Table 1, the Ni-, Cu-, Ru-, Rh-, Pd-, Ag-, Os-, Ir-, and Pt-phosphorene systems exhibit nonmagnetic states, while the Fe-, Co-, and Au-phosphorene systems have the magnetic moments of 2, 1, and 0.96 μ_B,

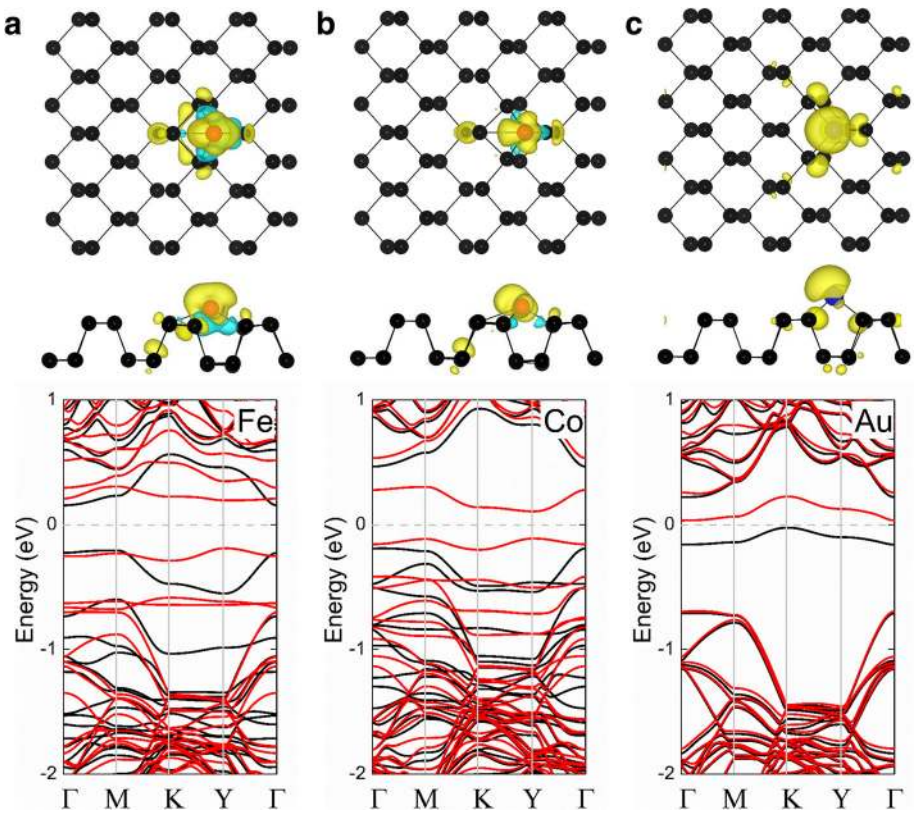

Fig. 2 Spin densities of the **a** Fe-phosphorene, **b** Co-phosphorene, and **c** Au-phosphorene systems are shown in the top row; the corresponding band structure of each system is shown at the bottom row. The black and red spheres represent P and TM atoms, respectively. In the top row, a plot of the spin-polarized charge density with a charge density iso-surface value of 0.002 e/Å^3 is superimposed on the top and side views of the crystal structure of pristine phosphorene for each of the TM-phosphorene systems; the yellow and cyan regions correspond to the up and down spins, respectively. In the plot of band structures (bottom row), the black and the red lines denote spin-up and spin-down channels, respectively; the Fermi level is set to zero, and it is indicated by the gray dashed line

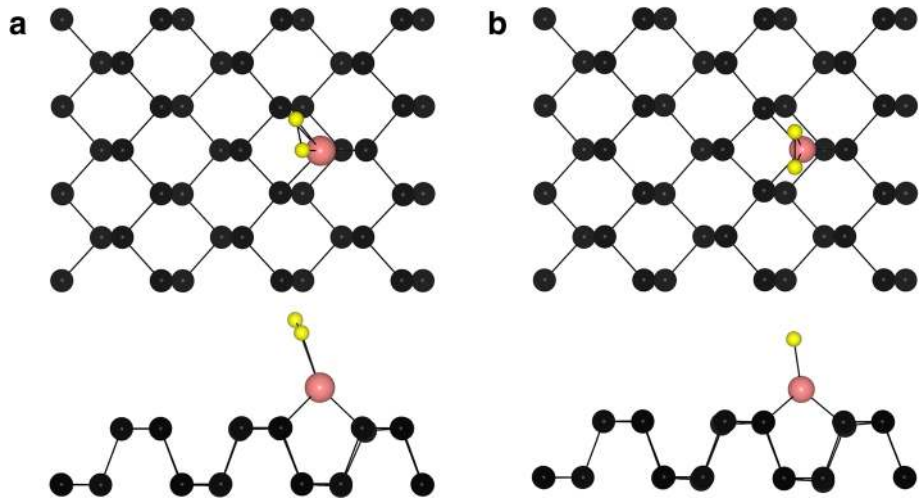

Fig. 3 Top and side views of typical adsorption sites of an O_2 molecule on TM-phosphorene. The black, pink, and yellow spheres represent P, TM, and O atoms, respectively

respectively. The spin-polarized charge density ($\rho = \rho_{\text{spin-up}} - \rho_{\text{spin-down}}$) is also shown in Fig. 2 to explore the origin and distribution of magnetism in the magnetic TM-phosphorene adsorption systems. The magnetic moment in each of these cases primarily originates from the adatom, with a small magnetic moment resulting from the nearest neighbors. Furthermore, the calculated band structures of the Fe-, Co-, and Au-phosphorene systems are depicted in Fig. 2. It can be seen that these systems are all magnetic semiconductors with bandgaps of 0.38, 0.22, and 0.06 eV, respectively, which are useful for spintronic applications.

Next, we studied the adsorption behavior of O_2 on top of the TM atom in the TM-phosphorene systems. Two typical energy-lowest configurations for the adsorption of O_2 on TM-phosphorene systems (O_2-(TM-phosphorene)) are shown in Fig. 3. For O_2-(Fe-phosphorene), O_2-(Co-phosphorene), O_2-(Cu-phosphorene), O_2-(Pd-phosphorene), and O_2-(Pt-phosphorene) systems, the O_2 molecule is parallel to the zigzag direction of phosphorene (Fig. 3a), with an O–P bond length of 1.84 Å, 1.86 Å, 2.04 Å, 2.18 Å, and 2.05 Å, respectively. For the O_2-(Ni-phosphorene), O_2-(Ru-phosphorene), O_2-(Rh-phosphorene), O_2-(Ag-phosphorene), O_2-(Os-phosphorene), O_2-(Ir-phosphorene), and O_2-(Au-phosphorene) systems, the molecule is along the zigzag direction of phosphorene (Fig. 3b), at a certain angle from the surface. Meanwhile, the two neighboring O atoms around the TM adatom are not equivalent. The results are displayed in Table 2. The adsorption energy (E_{ad}) of O_2 on an O_2-(TM-phosphorene) system was calculated as:

$$E_{\text{ad}} = E_{\text{TM-phosphorene}} + E_{\text{O}^2} - E_{\text{O}^2\text{-TM-phosphorene}} \quad (2)$$

where $E_{\text{O}^2\text{-TM-phosphorene}}$, $E_{\text{TM-phosphorene}}$, and E_{O^2} are the total energies of the O_2-(TM-phosphorene) system, the TM-phosphorene system, and the O_2 molecule, respectively. As shown in Table 2, the adsorption energies are 2.659, 1.850, 0.970, 0.906, 2.402, 1.548, 0.001, 0.786, 3.109, 1.980, 0.416, and 1.029 eV for the O_2-(Fe-phosphorene), O_2-(Co-phosphorene), O_2-(Ni-phosphorene), O_2-(Cu-phosphorene), O_2-(Ru-phosphorene), O_2-(Rh-phosphorene), O_2-(Pd-phosphorene), O_2-(Ag-phosphorene), O_2-(Os-phosphorene), O_2-(Ir-phosphorene), O_2-(Pt-phosphorene), and O_2-(Au-phosphorene) systems, respectively. In all cases, the large adsorption energies

Table 2 Parameters of O_2-(TM-phosphorene) adsorption systems: adsorption energy, charge transferred (*C*) from TM-phosphorene to the O_2 molecule, and calculated bond lengths of O–O and O–TM

Dopant	E_{ad} (eV)	*C* (e)	Bond length (Å)		
			($d_{\text{O-O}}$)	($d_{\text{O1-TM}}$)	($d_{\text{O2-TM}}$)
Fe	2.659	− 0.68	1.38	1.84	1.84
Co	1.850	− 0.50	1.36	1.86	1.86
Ni	0.970	− 0.42	1.32	2.14	1.90
Cu	0.906	− 0.52	1.35	2.04	2.04
Ru	2.402	− 0.46	1.40	1.91	2.08
Rh	1.548	− 0.24	1.34	2.07	2.03
Pd	0.001	− 0.24	1.32	2.18	2.18
Ag	0.786	− 0.37	1.30	2.19	2.98
Os	3.109	− 0.53	1.46	2.04	1.92
Ir	1.980	− 0.25	1.39	2.00	2.06
Pt	0.416	− 0.19	1.40	2.05	2.05
Au	1.029	− 0.09	1.32	2.12	2.93

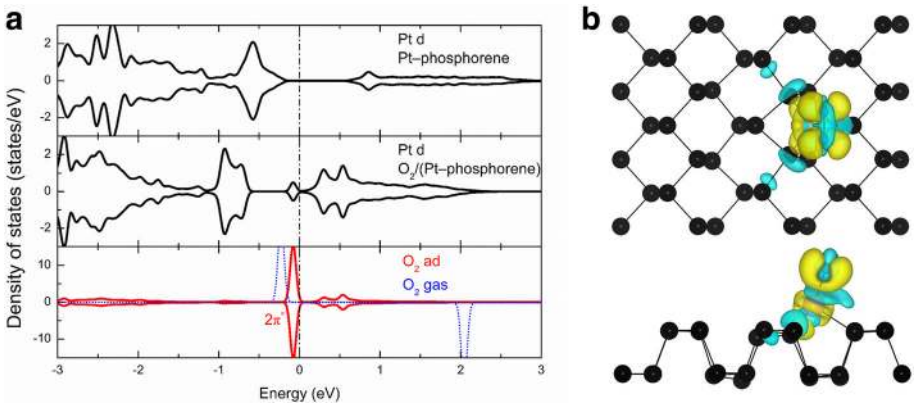

Fig. 4 **a** Local density of states (LDOS) of Pt and O_2 molecules in Pt-phosphorene and O_2-Pt-phosphorene systems and gas phase O_2, respectively. **b** Charge density difference in the O_2-(Pt-phosphorene) system; the yellow region (i.e., + 0.002 e/Å^3) and the cyan region (i.e., – 0.002 e/Å^3) correspond to the increase and the loss, respectively, of the electron density

except for that of the O_2-(Pd-phosphorene) system indicate that O_2 is chemisorbed.

It is fairly recognized that the elongation of the O–O bond is crucial for both Langmuir-Hinshelwood and Eley-Rideal mechanisms of a catalyst in the oxidation of CO [57]. Generally speaking, the longer the O–O bond length, the easier the catalyst reaction. The O–O and TM–O bond lengths in each system are also shown in Table 2. Obviously, the O–O bond increases from 1.23 Å for the pristine O_2 molecule to 1.38, 1.36, 1.32, 1.35, 1.40, 1.34, 1.32, 1.30, 1.46, 1.39, 1.40, and 1.32 Å, respectively, for the adsorbed molecule, possibly because O_2 is an electron acceptor. Furthermore, the bond length of TM–O in most O_2-(TM-phosphorene) systems is short owing to the interaction between O_2 and the TM atoms. This bond length varies from 1.84 to 2.19 Å and results in the formation of chemical bonds. In particular, the O–O bond is elongated to 1.40 Å, the highest value among the systems, in the adsorbed O_2 molecule on the Pt-phosphorene system. Thus, the Pt-phosphorene system is quite suitable as a catalyst for the oxidation of CO because it probably has the high catalytic ability.

Table 3 Calculated total magnetic moment (M_{total}) of O_2-(TM-phosphorene) systems. The magnetic moments of impurity atoms (M_{TM}) and an oxygen molecule (M_{O^2}) are also shown for comparison

Dopant	M_{total} (μ_B)	M_{TM}	M_{O^2}
Fe	2.00	1.43	0.51
Co	1.00	0.47	0.44
Ni	2.00	0.49	1.33
Cu	1.00	0.02	1.09
Rh	1.00	0.18	0.76
Ag	1.14	– 0.01	1.33
Ir	1.00	0.27	0.49
Au	1.00	0.00	1.02

In order to obtain more insight into the underlying mechanism of the high activity of these systems, we selected O_2-(Pt-phosphorene) as an example and investigated its local density of states (LDOS). Figure 4a shows the LDOS projected onto d orbitals of Pt in the Pt-phosphorene system, d orbitals of Pt in the O_2-(Pt-phosphorene) system, the O–O bond in the O_2-(Pt-phosphorene) system, and the gas phase O_2. In the upper panel of Fig. 4a, one peak can be seen at E_F – 0.6 eV, which originates from the partially occupied d orbital of Pt in the Pt-phosphorene system. These states should be responsible for the high activity of the Pt-phosphorene system. After the adsorption of an O_2 molecule, the LDOS projected onto d orbitals of Pt below the Fermi level is downshifted after the adsorption of the O_2 molecule owing to the charge transfer, and the states above the Fermi level is also substantially increased. Meanwhile, the LDOS projected onto the adsorbed O_2 molecule indicates that the O_2 $2\pi^*$ orbitals (lowest unoccupied molecular orbital, LUMO) are becoming partially occupied, which has downshifted from its gas value of E_F + 2 eV to E_F – 0.1 eV. For clarification, the charge density difference of the O_2-(Pt-phosphorene) system is also presented.

The charge density difference is defined as follows:

$$\Delta_\rho = \rho_T - \rho_{\text{molecule}} - \rho_{\text{absorbed}} \quad (3)$$

where ρ_T, ρ_{molecule}, and ρ_{absorbed} are the total charges on the O_2-(Pt-phosphorene) system, O_2 molecule, and the Pt-phosphorene system, respectively. As shown in Fig. 4b, the large yellow region localized on the O_2 molecule indicates that there is a significant electron transfer from Pt-phosphorene to O_2, which also indicates the strong orbital hybridization between O_2 and the Pt-phosphorene system.

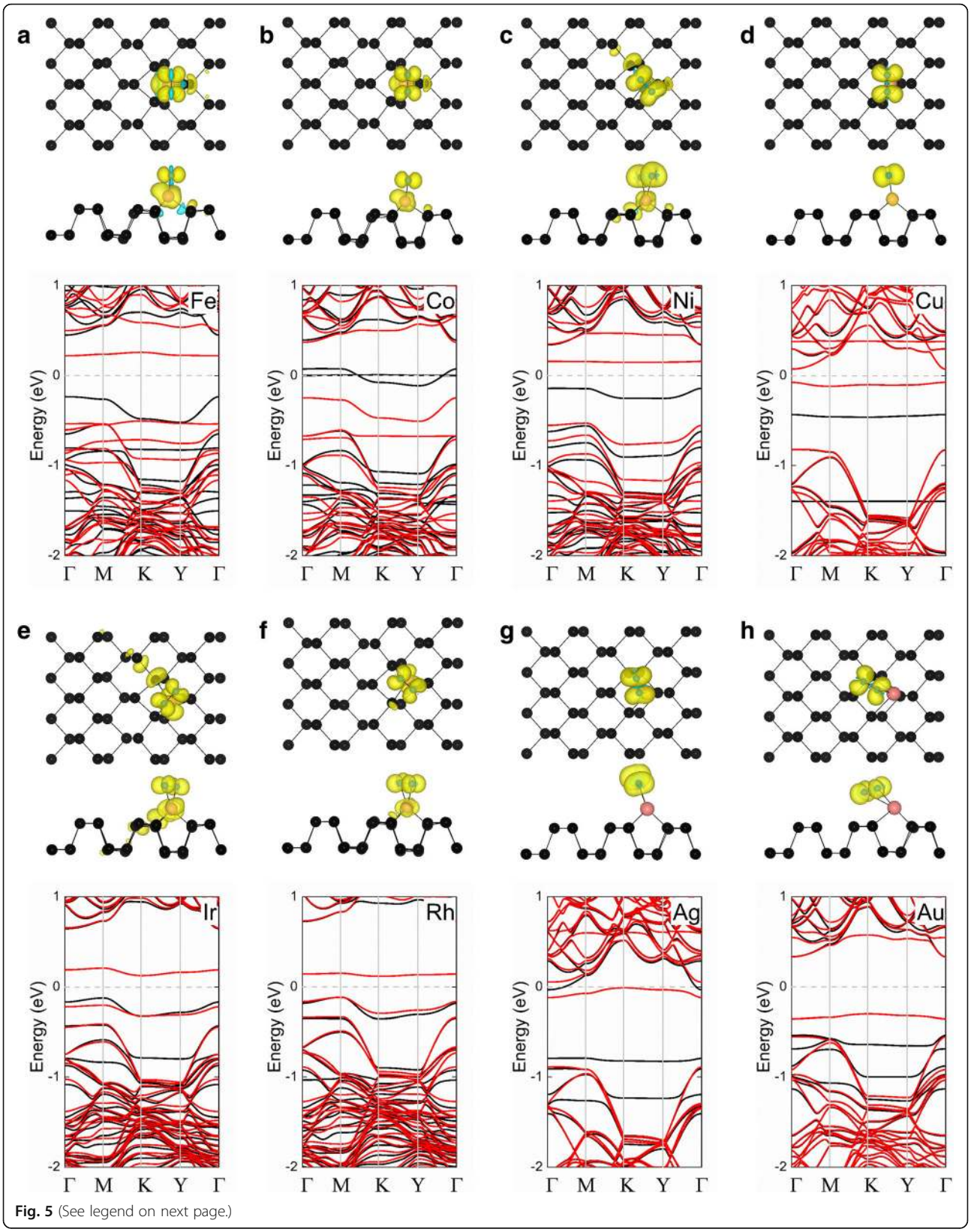

Fig. 5 (See legend on next page.)

(See figure on previous page.)
Fig. 5 Spin densities of the **a** O_2-(Fe-phosphorene), **b** O_2-(Co-phosphorene), **c** O_2-(Ni-phosphorene), **d** O_2-(Cu-phosphorene), **e** O_2-(Ir-phosphorene), **f** O_2-(Rh-phosphorene), **g** O_2-(Ag-phosphorene), and **h** O_2-(Au-phosphorene) systems are shown in the top row; the corresponding band structure of each system is shown in the bottom row. In the top row, a plot of the spin-polarized charge density with a charge density iso-surface value of 0.002 e/Å^3 is superimposed on the top and side views of the crystal structure of pristine phosphorene; the yellow and cyan regions correspond to up and down spins, respectively. In the plots of band structures, the black and the red lines denote spin-up and spin-down channels, respectively; the Fermi level is set to zero, and it is indicated by the gray dashed line

According to the Bader charge analysis [54–56], 0.19|e| is transferred from the Pt-phosphorene system to the O_2 molecule. Therefore, the large charge transfer fills the antibonding states of the O_2 molecule and significantly weakens the O–O bond. Similarly, the underlying mechanism of the high activity of other systems can also be understood by the charge transfer between the O_2 molecule and the TM-phosphorene system. Indeed, Bader charge analysis [54–56] showed that charges of − 0.68, − 0.50, − 0.42, − 0.52, − 0.46, − 0.24, − 0.24, − 0.37, − 0.53, − 0.25, − 0.19, and − 0.09|e| are transferred from TM-phosphorene to the oxygen molecule in the O_2-(Fe-phosphorene), O_2-(Co-phosphorene), O_2-(Ni-phosphorene), O_2-(Cu-phosphorene), O_2-(Ru-phosphorene), O_2-(Rh-phosphorene), O_2-(Pd-phosphorene), O_2-(Ag-phosphorene), O_2-(Os-phosphorene), O_2-(Ir-phosphorene), O_2-(Pt-phosphorene), and O_2-(Au-phosphorene) systems, respectively.

Finally, we studied the magnetic properties of O_2-(TM-phosphorene) systems. The magnetic moments of the O_2-(TM-phosphorene) systems are shown in Table 3. The O_2-(Ni-phosphorene), O_2-(Cu-phosphorene), O_2-(Rh-phosphorene), O_2-(Ag-phosphorene), and O_2-(Ir-phosphorene) systems have magnetic moments of 2.00, 1.00, 1.00, 1.14, and 1.00 μ_B, respectively, which all result from the adsorption of a paramagnetic O_2 molecule. The spin-polarized charge density of these O_2-(TM-phosphorene) systems is displayed in Fig. 5. For the O_2-(Fe-phosphorene) and O_2-(Co-phosphorene) systems, the magnetic moment is believed to mainly arise from the transition metal atom and the O_2 molecule. On the contrary, for the O_2-(Ni-phosphorene), O_2-(Cu-phosphorene), O_2-(Rh-phosphorene), O_2-(Ag-phosphorene), O_2-(Ir-phosphorene), and O_2-(Au-phosphorene) systems, the magnetic moment mainly comes from the O_2 molecule. These hypotheses are consistent with the results displayed in Table 3. To better comprehend how the adsorption of a gas molecule affects the electronic structure of the O_2-(TM-phosphorene) system, the electronic band structures of each system was calculated, and the results are shown in Fig. 5. First, we discovered that a flat band occurs around the Fermi level (E_F) after the adsorption of O_2 molecule in all systems, which primarily from the O_2 molecule. For the O_2-(Fe-phosphorene), O_2-(Co-phosphorene), O_2-(Ni-phosphorene), O_2-(Cu-phosphorene), O_2-(Rh-phosphorene), O_2-(Ir-phosphorene), O_2-(Ag-phosphorene), and O_2-(Au-phosphorene) systems, the channels for spin-up and spin-down split reveal the magnetic characteristics. The O_2-(Fe-phosphorene), O_2-(Ni-phosphorene), O_2-(Cu-phosphorene), O_2-(Ir-phosphorene), O_2-(Rh-phosphorene), O_2-(Ag-phosphorene), and O_2-(Au-phosphorene) exhibit magnetic semiconducting behavior, with a considerable bandgap except for the O_2-(Co-phosphorene) system, which was revealed to be half-metallic. These results suggest that the systems have the potential for application in phosphorene-based spintronics.

Conclusions

We investigated the structural, electronic, and magnetic properties of different TM-phosphorene systems. All the adatoms were found to prefer to occupy the hollow site on phosphorene. The considerable adsorption energy reveals that all of the TM-phosphorene adsorption systems are rather robust, indicating that phosphorene forms strong bonds with all 12 types of TM adatoms. Furthermore, we found that doping with Fe, Co, and Au can result in magnetic semiconducting properties in monolayered phosphorene, with total magnetic moments of 2, 1, and 0.96 μ_B, respectively.

In addition, we also examined the properties of an O_2 molecule adsorbed on the TM-phosphorene system. It was very encouraging to find that all of the O_2-(TM-phosphorene) systems, except for O_2-(Pd-phosphorene), display good catalytic activity for the oxidation of CO owing to the elongation of the O–O bond. The O_2-(Fe-phosphorene), O_2-(Ni-phosphorene), O_2-(Cu-phosphorene), O_2-(Rh-phosphorene), O_2-(Ag-phosphorene), O_2-(Ir-phosphorene), and O_2-(Au-phosphorene) systems display spin-polarized semiconducting properties with magnetic moments of 2.00, 2.00, 1.00, 1.00, 1.14, 1.00, and 1.00 μ_B. The O_2-(Co-phosphorene) displays magnetic half-metallic characteristics, with a magnetic moment of 2.00 μ_B. Therefore, our results may open new possibilities for applying phosphorene in the fields of catalysis and spintronics.

Abbreviations

2D: Two-dimensional; B: Bridge; GGA: Generalized gradient approximation; H: Hollow site; LDOS: Local density of states; PBE: Perdew-Burke-Ernzerh; T: Top of a phosphorus atom; TM: Transition metal

Funding

This work was supported by the National Natural Science Foundation of China (No. 51731004, No. 51675100, No. 11864047), the National Science

Foundation for Young Scientists of China (No. 11704165), the Science Foundation of Jinling Institute of Technology (No. 40620064), the Science Foundation of Guizhou Science and Technology Department (No. QKHJZ[2015]2150), and the Science Foundation of Guizhou Provincial Education Department (No. QJHKYZ[2016]092). First-principles calculations were carried out on the Yu Jin's group clusters at the Southeast University.

Availability of Data and Materials
They are all in the main text and figures.

Authors' Contributions
JY and MS design the project. YL and MS wrote the manuscript. All the authors discussed the results. All authors read and approved the final manuscript.

Competing Interests
The authors declare that they have no competing interests.

Publisher's Note

Author details
[1]Jiangsu Key Laboratory of Advanced Metallic Materials, School of Materials Science and Engineering, Southeast University, Nanjing 211189, Jiangsu, People's Republic of China. [2]Department of Physics, Zunyi Normal College, Zunyi 563002, Guizhou, People's Republic of China. [3]Department of Fundamental Courses, Jinling Institute of Technology, Nanjing 211169, Jiangsu, People's Republic of China. [4]School of Mechanical Engineering, Southeast University, Nanjing 211189, Jiangsu, People's Republic of China. [5]Institute of High Performance Computing, A*STAR, Singapore 138632, Singapore.

Received: 26 July 2018 Accepted: 29 August 2018
Published online: 12 September 2018

References
1. Li L, Yu Y, Ye GJ, Ge Q, Ou X, Wu H, Feng D, Chen XH, Zhang Y (2014) Black phosphorus field-effect transistors. Nat Nano 9(5):372–379.
2. Liu H, Neal AT, Zhu Z, Luo Z, Xu XF, Tománek D, Ye PD (2014) Phosphorene: an unexplored 2D semiconductor with a high hole mobility. ACS Nano 8(4): 4033–4041.
3. Chowdhury C, Datta A (2017) Exotic physics and chemistry of two-dimensional phosphorus: phosphorene. J Phys Chem Lett 8(13):2909–2916.
4. Cai Y, Zhang G, Zhang Y (2014) Layer-dependent band alignment and work function of few-layer phosphorene. Sci Rep 4:6677.
5. Qiao JS, Kong XH, Hu ZX, Y F JW (2014) High-mobility transport anisotropy and linear dichroism in few-layer black phosphorus. Nat Commun 5:4475.
6. Xiao J, Long MQ, Zhang XJ, Ouyang J, Xu H, Gao YL (2015) Theoretical predictions on the electronic structure and charge carrier mobility in 2D phosphorus sheets. Sci Rep 5:9961.
7. Wei Q, Peng XH (2014) Superior mechanical flexibility of phosphorene and few-layer black phosphorus. Appl Phys Lett 104(25):251915.
8. Fei R, Faghaninia A, Soklaski R, Yan JA, Lo C, Yang L (2014) Enhanced thermoelectric efficiency via orthogonal electrical and thermal conductances in phosphorene. Nano Lett 14(11):6393–6399.
9. Ong Z, Cai Y, Zhang G, Zhang YW (2014) Strong thermal transport anisotropy and strain modulation in single-layer phosphorene. J Phys Chem C 118(43):25272–25277.
10. Cai YQ, Ke QQ, Zhang G, Feng YP, Shenoy VB, Zhang YW (2015) Giant phononic anisotropy and unusual anharmonicity of phosphorene: interlayer coupling and strain engineering. Adv Funct Mater 25(15):2230–2236.
11. Du YC, Liu H, Deng YX, Ye PD (2014) Device perspective for black phosphorus field-effect transistors: contact resistance, ambipolar behavior, and scaling. ACS Nano 8(10):10035–10042.
12. Na J, Lee YT, Lim JA, Hwang DK, Kim GT, Choi WK, Song YW (2014) Few-layer black phosphorus field-effect transistors with reduced current fluctuation. ACS Nano 8(11):11753–11762.
13. Avsar A, Vera-Marun IJ, Tan JY, Watanabe KJ, Taniguchi TS, Castro Neto AH, Özyilmaz B (2015) Air-stable transport in graphene-contacted, fully encapsulated ultrathin black phosphorus-based field-effect transistors. ACS Nano 9(4):4138–4145.
14. Kamalakar MV, Madhushankar BN, Dankert A, Dash SP (2015) Low Schottky barrier black phosphorus field-effect devices with ferromagnetic tunnel contacts. Small 11(18):2209–2216.
15. Zhu WN, Yogeesh MN, Yang SX, Aldave SH, Kim JS, Sonde S, Tao L, Ns L, Akinwande DJ (2015) Flexible black phosphorus ambipolar transistors, circuits and AM demodulator. Nano Lett 15(3):1883–1890.
16. Jeon PJ, Lee YT, Lim JY, Kim JS, Hwang DK, Im S (2016) Black phosphorus-zinc oxide nanomaterial heterojunction for p-n diode and junction field-effect transistor. Nano Lett 16(2):1293–1298.
17. Zhao S, Kang W, Xue J (2014) The potential application of phosphorene as an anode material in Li-ion batteries. J Mater Chem A 2(44):19046–19052.
18. Li W, Yang Y, Zhang G, Zhang YW (2015) Ultrafast and directional diffusion of lithium in phosphorene for high-performance lithium-ion battery. Nano Lett 15(3):1691–1697.
19. Sun J, Lee H, Pasta M, Yuan HT, Zheng GY, Sun YM, Li YZ, Cui Y (2015) A phosphorene-graphene hybrid material as a high-capacity anode for sodium-ion batteries. Nat Nano 10:980.
20. Zhou L, Zhang J, Zhuo Z, Kou LZ, Ma W, Shao B, Du AJ, Meng S, Frauenheim T (2016) Novel excitonic solar cells in phosphorene-TiO2 heterostructures with extraordinary charge separation efficiency. J Phys Chem Lett 7(10):1880–1887.
21. Hu W, Lin L, Yang C, Dai J, Yang JL (2016) Edge-modified phosphorene nanoflake heterojunctions as highly efficient solar cells. Nano Lett 16(3): 1675–1682.
22. Rahman MZ, Kwong CW, Davey K, Qiao SZ (2016) 2D phosphorene as a water splitting photocatalyst: fundamentals to applications. Energy Environ Sci 9(3):709–728.
23. Babar R, Kabir M (2016) Transition metal and vacancy defect complexes in phosphorene: a spintronic perspective. J Phys Chem C 120(27):14991–15000.
24. Cai Y, Ke Q, Zhang G, Zhang YW (2015) Energetics, charge transfer, and magnetism of small molecules physisorbed on phosphorene. J Phys Chem C 119(6):3102–3110.
25. Abbas AN, Liu B, Chen L, Ma YQ, Cong S, Aroonyadet N, Köpf M, Nilges T, Zhou CW (2015) Black phosphorus gas sensors. ACS Nano 9(5):5618–5624.
26. Cui S, Pu H, Wells SA, Wen ZH, Mao S, Chang JB, Hersam MC, Chen JH (2015) Ultrahigh sensitivity and layer-dependent sensing performance of phosphorene-based gas sensors. Nat Commun 6:8632.
27. Cao C, Wu M, Jiang J, Jiang JZ, Cheng HP (2010) Transition metal adatom and dimer adsorbed on graphene: induced magnetization and electronic structures. Phys Rev B 81(20):205424.
28. Kaloni TP, Singh N, Schwingenschlögl U (2014) Prediction of a quantum anomalous hall state in co-decorated silicene. Phys Rev B 89(3):035409.
29. Ersan F, Aktürk E, Ciraci S (2016) Interaction of adatoms and molecules with single-layer arsenene phases. J Phys Chem C 120(26):14345–14355.
30. Kulish VV, Malyi OI, Persson C, Wu P (2015) Adsorption of metal adatoms on single-layer phosphorene. Phys Chem Chem Phys 17(2):992–1000.
31. Ding Y, Wang Y (2015) Structural, electronic, and magnetic properties of adatom adsorptions on black and blue phosphorene: a first-principles study. J Phys Chem C 119(19):10610–10622.
32. Hu T, Hong J (2015) First-principles study of metal adatom adsorption on black phosphorene. J Phys Chem C 119(15):8199–8207.
33. Li C, Yang S, Li S, Li SS, Xia JB, Li JB (2013) Au-decorated silicene: design of a high-activity catalyst toward CO oxidation. J Phys Chem C 117(1):483–488.
34. Qiao B, Wang A, Yang X, Allard LF, Jiang Z, Cui YT, Liu JY, Li J, Zhang T (2011) Single-atom catalysis of CO oxidation using Pt_1/FeO_x. Nat Chem 3:634.
35. Green IX, Tang WJ, Neurock M, Yates JT (2011) Spectroscopic observation of dual catalytic sites during oxidation of CO on a Au/TiO_2 catalyst. Science 333(6043):736–739.
36. Matthey D, Wang JG, Wendt S, Matthiesen J, Schaub R, Laegsgaard E, Hammer B, Besenbacher F (2007) Enhanced bonding of gold nanoparticles on oxidized TiO_2(110). Science 315(5819):1692–1696.
37. Langmuir I (1922) The mechanism of the catalytic action of platinum in the reactions $2CO + O_2 = 2CO_2$ and $2H_2 + O_2 = 2H_2O$. Trans Faraday Soc 17(0): 621–654.
38. Lopez-Acevedo O, Kacprzak KA, Akola J, Häkkinen HN (2010) Quantum size effects in ambient CO oxidation catalysed by ligand-protected gold clusters. Nat Chem 2:329.
39. Haruta M (2011) Spiers memorial lecture role of perimeter interfaces in catalysis by gold nanoparticles. Faraday Discuss 152(0):11–32.

40. Yang Y, Rigdon W, Huang XY, Li XD (2013) Enhancing graphene reinforcing potential in composites by hydrogen passivation induced dispersion. Sci Rep 3:2086.
41. Over H, Kim YD, Seitsonen AP, Wendt S, Lundgren E, Schmid M, Varga P, Morgante A, Ertl G (2000) Atomic-scale structure and catalytic reactivity of the RuO_2(110) surface. Science 287(5457):1474–1476.
42. Yoon B, Häkkinen H, Landman U, Worz AS, Antonietti JM, Abbet S, Judai K, Heiz U (2005) Charging effects on bonding and catalyzed oxidation of CO on Au_8 clusters on MgO. Science 307(5708):403–407.
43. Oh S, Hoflund GB (2007) Low-temperature catalytic carbon monoxide oxidation over hydrous and anhydrous palladium oxide powders. J Catal 245(1):35–44.
44. Gustafson J, Westerström R, Balmes O, Resta A, van Rijn R, Torrelles X, Herbschleb CT, Frenken JWM, Lundgren E (2010) Catalytic activity of the Rh surface oxide: CO oxidation over Rh(111) under realistic conditions. J Phys Chem C 114(10):4580–4583.
45. Joo SH, Park JY, Renzas JR, Butcher DR, Huang WY, Somorjai GA (2010) Size effect of ruthenium nanoparticles in catalytic carbon monoxide oxidation. Nano Lett 10(7):2709–2713.
46. Kresse G, Furthmüller J (1996) Efficiency of ab-initio total energy calculations for metals and semiconductors using a plane-wave basis set. Comput Mater Sci 6(1):15–50.
47. Kresse G, Furthmüller J (1996) Efficient iterative schemes for ab initio total-energy calculations using a plane-wave basis set. Phys Rev B 54(16):11169–11186.
48. Perdew JP, Burke K, Ernzerhof M (1996) Generalized gradient approximation made simple. Phys Rev Lett 77(18):3865–3868.
49. Perdew JP, Burke K, Ernzerhof M (1997) Generalized gradient approximation made simple [Phys. Rev. Lett. 77, 3865 (1996)]. Phys Rev Lett 78(7):1396.
50. Kresse G, Joubert D (1999) From ultrasoft pseudopotentials to the projector augmented-wave method. Phys Rev B 59(3):1758–1775.
51. Grimme S, Antony J, Ehrlich S, Krieg H (2010) A consistent and accurate ab initio parametrization of density functional dispersion correction (DFT-D) for the 94 elements H-Pu. J Chem Phys 132(15):154104.
52. Monkhorst HJ, Pack JD (1976) Special points for Brillouin-zone integrations. Phys Rev B 13(12):5188–5192.
53. Chowdhury C, Jahiruddin S, Datta A (2016) Pseudo-Jahn-teller distortion in two-dimensional phosphorus: origin of black and blue phases of phosphorene and band gap modulation by molecular charge transfer. J Phys Chem Lett 7(7):1288–1297.
54. Sanville E, Kenny SD, Smith R, Henkelman G (2007) Improved grid-based algorithm for Bader charge allocation. J Comput Chem 28(5):899–908.
55. Henkelman G, Arnaldsson A, Jónsson H (2006) A fast and robust algorithm for Bader decomposition of charge density. Comput Mater Sci 36(3):354–360.
56. Tang W, Sanville E, Henkelman G (2009) A grid-based Bader analysis algorithm without lattice bias. J Phys Condens Matter 21(8):084204.
57. Karmakar S, Chowdhury C, Datta A (2018) Noble-metal-supported GeS monolayer as promising single-atom catalyst for CO oxidation. J Phys Chem C 122(26):14488–14498.